

Chirality-Selective Excitation of Coherent Phonons in Carbon Nanotubes by Femtosecond Optical Pulses

J.-H. Kim,¹ K.-J. Han,¹ N.-J. Kim,¹ K.-J. Yee,^{1,*} Y.-S. Lim,² G. D. Sanders,³
C. J. Stanton,³ L. G. Booshehri,⁴ E. H. H  roz,⁴ and J. Kono^{4,†}

¹*Department of Physics, Chungnam National University, Daejeon, 305-764, Republic of Korea*

²*Department of Applied Physics, Konkuk University, Chungju, Chungbuk, 380-701, Republic of Korea*

³*Department of Physics, University of Florida, Gainesville, Florida 32611, USA*

⁴*Department of Electrical and Computer Engineering, Rice University, Houston, Texas 77005, USA*

(Dated: February 2, 2022)

Using pre-designed trains of femtosecond optical pulses, we have selectively excited coherent phonons of the radial breathing mode of specific-chirality single-walled carbon nanotubes within an ensemble sample. By analyzing the initial phase of the phonon oscillations, we prove that the tube diameter initially increases in response to ultrafast photoexcitation. Furthermore, from excitation profiles, we demonstrate that an excitonic absorption peak of carbon nanotubes periodically oscillates as a function of time when the tube diameter undergoes radial breathing mode oscillations.

PACS numbers: 78.67.Ch, 71.35.Ji, 78.55.-m

Single-walled carbon nanotubes (SWNTs), hollow one-dimensional nanostructures with unique electronic, mechanical, and optical properties, come in a variety of species, or chiralities. Some of them are metallic and others semiconducting, depending on their chiral indices (n, m) [1, 2, 3]. This diversity, while making them such unusual nanomaterials, often makes it challenging to extract reliable parameters on chirality-dependent properties from experimental results on ensemble samples. Currently, there are world-wide efforts on SWNT purification, separation, and enrichment, producing promising results [4, 5, 6, 7, 8]. However, a standard for fabrication of these samples has yet to be established.

Here, we present a novel method that allows us to study single-chirality nanotubes even though the sample contains nanotubes of many different chiralities. Specifically, we have utilized the techniques of femtosecond pulse shaping [9, 10, 11] in ultrafast pump-probe spectroscopy of SWNTs to selectively excite the coherent lattice vibrations [12, 13] of the radial breathing mode (RBM) of specific chiralities. The excitation spectra of such coherent phonons (CPs) provide chirality-specific information on the processes of light absorption, phonon generation, and phonon-induced band structure modulations in unprecedented detail. In particular, the excitation-energy-dependence of the phase of the CP oscillations provides direct, time-domain evidence that band gap oscillations follow the diameter oscillations in the RBM coherent phonon mode.

The sample studied was a micelle-suspended SWNT solution, where the SWNTs (HiPco batch HPR 104) were suspended as individuals with sodium cholate [14]. The optical setup was that of standard degenerate pump-probe spectroscopy, but chirality selectivity was achieved by using multiple pulse trains, with a pulse-to-pulse interval corresponding to the period of a specific RBM mode. Among different species of nanotubes, those hav-

ing RBM frequencies that are matched to the repetition rate of multiple pulse trains will generate large amplitude coherent oscillations with increasing oscillatory response to each pulse, while others will have diminished coherent responses [15, 16, 17]. The tailoring of multiple pulse trains from femtosecond pulses was achieved using the pulse-shaping technique described elsewhere [10]. Pulse trains are incident on an ensemble of nanotubes as a pump beam, and coherent RBM oscillations are monitored by an unshaped, Gaussian probe beam. The pump pulse fluence was around 4×10^{-6} J/cm², where no noticeable change in the RBM frequency or in the decay rate was observed when the pump fluence was adjusted.

The strength of our pulse-shaping technique is shown in Fig. 1. Real-time observation of coherent RBM oscillations is possible without pulse-shaping by employing standard femtosecond pump-probe spectroscopy [12, 13]. Figure 1(a) shows transmission modulations of the probe beam induced by coherent phonon lattice vibrations, which were generated by pump pulses with a pulse-width of 50 fs and a central wavelength of 800 nm. The time-domain beating profiles reflect the simultaneous generation of several RBM frequencies [12], which are clearly seen in the Fourier-transform of the time-domain data in the right of Fig. 1(a). Although resonance conditions and RBM frequencies lead to the assignment of peaks to their corresponding chiralities, obtaining detailed information on dynamical quantities such as the phase information of phonon oscillations becomes rather challenging. Additionally, if adjacent phonon modes overlap in the spectral domain, this can lead to peak distortions.

However, by introducing pulse-shaping, multiple pulses with different repetition rates are used to excite RBM oscillations, and, as shown in Figs. 1(b)-1(e), chirality selectivity was successfully obtained. With the appropriate repetition rate of the pulse trains, a single, specific chirality dominantly contributes to the signal, while other

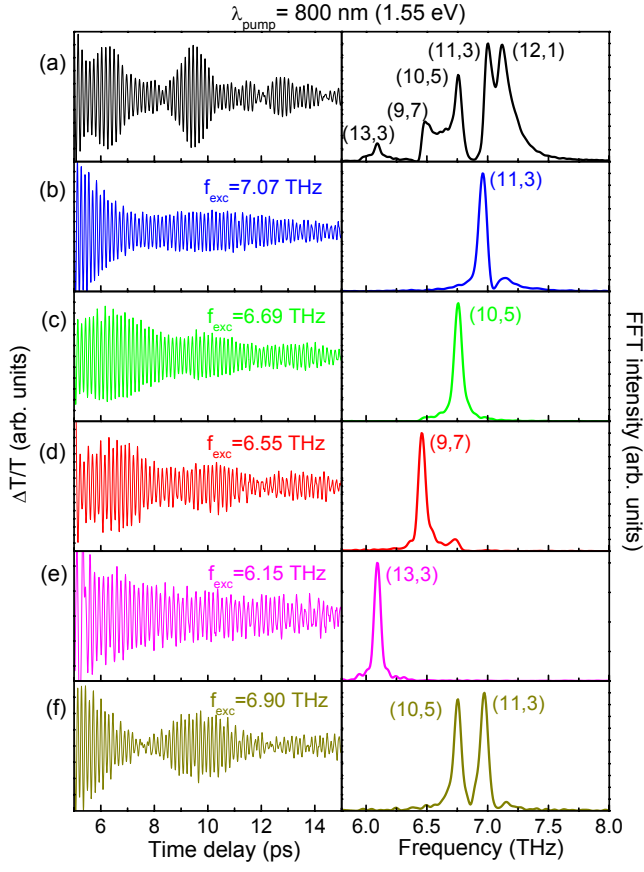


FIG. 1: (color online). (a): (Left) Time-domain transmission modulations due to coherent RBM vibrations in ensemble SWNT solution generated using standard pump-probe techniques *without* pulse shaping; (Right) Fourier transformation of time-domain oscillations with chirality assigned peaks. (b-f): (Left) Time-domain coherent RBM oscillations selectively excited by multiple pulse trains via pulse shaping with corresponding repetition rates of 7.07-6.15 THz; (Right) Fourier transformations of corresponding oscillations, with their dominant nanotube chirality (n,m) indicated. In (f), the pump repetition rate was intentionally tuned to the middle of the RBM frequencies for (11,3) and (10,5) nanotubes.

nanotubes are suppressed. For example, by choosing a pump repetition rate of 7.07 THz, we can selectively excite only the (11,3) nanotubes, as seen in Fig. 1(b). Similarly, with a pump repetition rate of 6.69 THz, the (10,5) nanotubes are selectively excited, as seen in Fig. 1(c). Finally, as demonstrated in Fig. 1(f), when the pump repetition rate was tuned to the middle of the RBM frequencies for (11,3) and (10,5) nanotubes, both nanotubes contributed. The accuracy of selectivity depends on the number of pulses in the tailored pulse train as well as on the distribution of chiralities in the nanotube ensemble. Furthermore, selective excitation of a specific chirality also requires the pump energy to be resonant with the corresponding second interband (or E_{22}) transition.

The ability to excite single-chirality tubes allows us

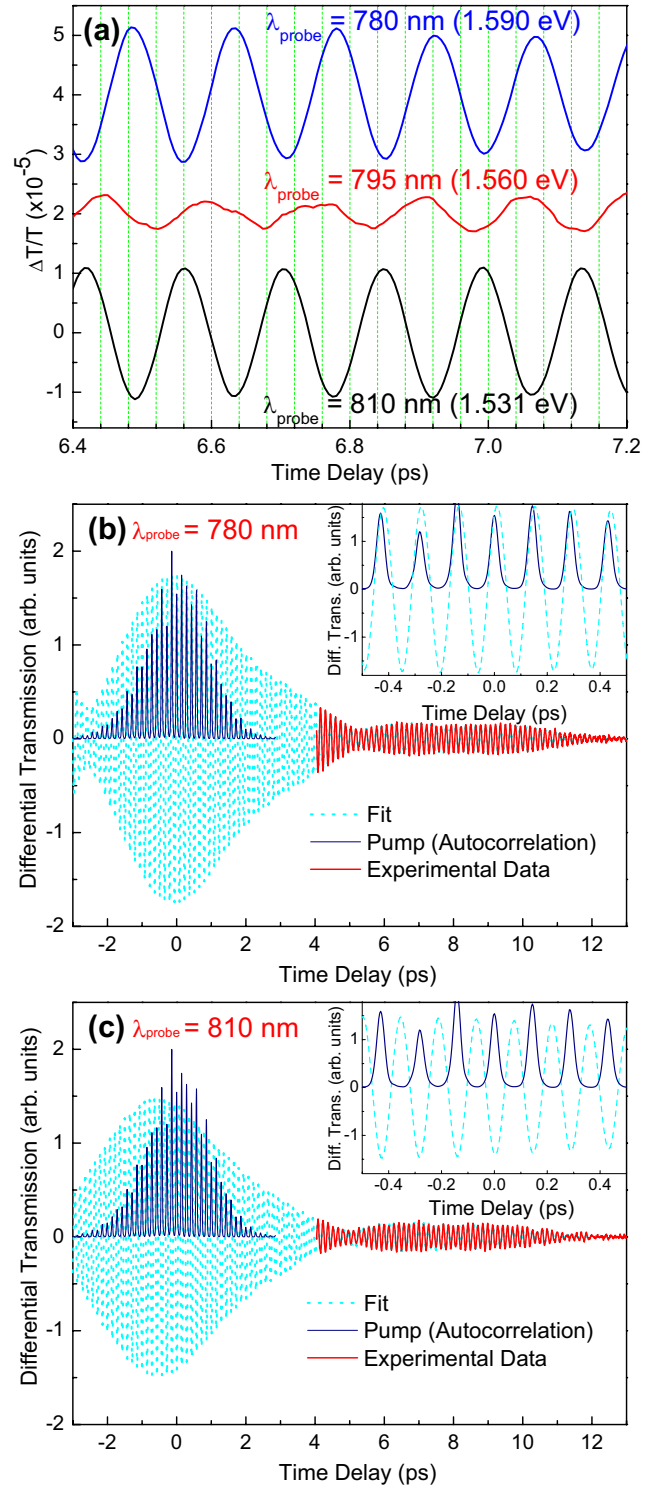


FIG. 2: (color online). (a) Differential transmission as a function of time delay at probe wavelengths of 780 nm, 795 nm, and 810 nm for the selective RBM excitation of the (11,3) nanotubes. There is a π phase shift between the 780 nm and 810 nm data. These three wavelengths correspond to below, at, and above the second exciton resonance, respectively, of (11,3) nanotubes. (b, c): Differential transmission as a function of time delay together with the pump pulse train as well as fit to exponentially-decaying sinusoidal oscillations.

to perform detailed studies of their excited states. For example, by placing a series of 10-nm band pass filters in the probe path before the detector, we can measure the wavelength-dependence of RBM-induced transmission changes to understand how the diameter change during RBM oscillations modifies the band structure. Figure 2(a) shows the differential transmission for three cases, corresponding to wavelengths below resonance, at resonance, and above resonance, respectively, for selectively-excited (11,3) nanotubes. Although the transmission is strongly modulated at the RBM frequency (6.96 THz) for all three cases, the amplitude and phase of oscillations vary noticeably for varying probe wavelengths. Specifically, the amplitude of oscillations becomes minimal at resonance, and, in addition, there is clearly a π -phase shift between the above- and below-resonance traces. Because the band gap energy and diameter are inversely related to each other in SWNTs [3], and because it is the RBM frequency at which the diameter is oscillating, we can conclude from this data that the energy of the E_{22} resonance is oscillating at the RBM frequency. Namely, when the band gap is decreasing, absorption above (below) resonance is decreasing (increasing), resulting in positive (negative) differential transmission.

We can also look at the short time response to see how the diameter changes in response to ultrafast photoexcitation of electron-hole pairs. In Fig. 2(b) and 2(c), we plot the differential transmission data taken at probe wavelengths above (a) and below (b) resonance together with the pump pulse train, with time zero corresponding to the center of the pulse train. The sign of the differential transmission oscillations in the first-quarter period is positive (negative) for the above (below) resonance probe, indicating that there is an initial decrease (increase) in absorption for above (below) resonance. Thus, this observation has an important implication for the nature of coherent phonon RBM diameter oscillations: the lattice must initially expand. This is an experimental observation that until now has not been verified, though theoretically predicted [18].

Our observations are supported by a microscopic theory we developed for the generation and detection of CP in SWNTs using an extended tight-binding model [19] to describe the nanotube electronic states and a valence force field model [20] to describe the phonons. We have examined trends in the CP spectra within and between mod 2 semiconducting nanotube families by plotting the theoretical CP intensity at the RBM phonon frequency as a function of pump/probe energy. This is done in the left panel of Fig. 3 where we plot our theoretical CP intensity at the RBM frequency as a function of pump/probe energy for all nanotubes in $2n + m$ Family 22 and 25. The curves for each nanotube are labeled with the nanotube chirality (n, m) and the RBM phonon energy in meV. In each nanotube, we see peaks in the CP spectra corresponding to E_{22} transitions. Within a given $2n + m$

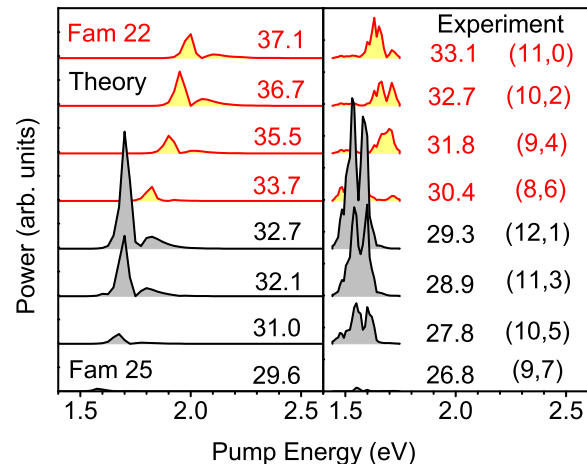


FIG. 3: (color online) Coherent phonon intensity at the RBM frequency as a function of pump/probe energy for several mod 2 semiconducting nanotubes at the E_{22} transition. Right: experimental spectra; left: simulated spectra. The upper four curves in each panel are for nanotubes in Family 22 and the lower four curves are for tubes in Family 25. Each curve is labeled with the chirality (n,m) and the RBM phonon energy in meV and offset for clarity.

family, the CP intensity tends to decrease as the chiral angle increases, i.e., as the chirality goes from $(n,0)$ zigzag tubes to (n,n) armchair tubes. From Fig. 3 we can also see that the theoretical CP intensity increases as we go from Family 22 to Family 25. The right panel of Fig. 3 shows the corresponding experimental CP spectra for the nanotubes in Families 22 and 25. Comparing experimental and theoretical curves in Fig. 3, we see that our theory correctly predicts the overall trends in the CP intensities both within and between families [21].

Considering the phase shift observed in Fig. 2, the amplitude of the differential transmission can be plotted as a function of probe energy, with the curve of the amplitude fit to the derivative of a Lorentzian function centered at 1.564 eV as seen in Fig. 4(a). The fitting to the derivative of a Lorentzian further supports the idea that modulating the absorption coefficient in time through CP and probing the change in transmission/reflection at various probe energies is essentially a type of modulation spectroscopy [22]. Similar, vibration-induced changes in absorption spectra have been observed in molecular systems [23]. As compared to previous CP experiments on SWNTs [12, 13], pulse-shaping offers phase information that causes the real time-domain data to be sensitive to the sign of the differential transmission, as the amplitude of the Lorentzian is largest at its inflection points [12]. In Fig. 4(b), the reconstructed Lorentzian corresponds to the excitation profile for coherent phonons, with a maximum peak comparable to the maximum position of the photoluminescence excitation profile for (11,3) nanotubes

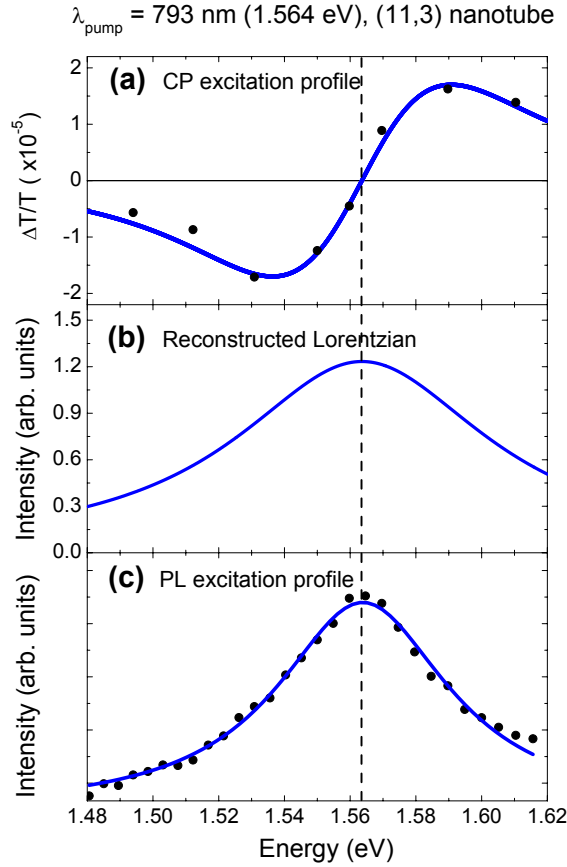


FIG. 4: (color online). Excitation profile of coherent phonons as evidence of band gap modulations. (a) Phonon amplitude as a function of probe energy fit to the derivative of a Lorentzian peak. (b) Lorentzian reconstructed from (a). (c) Photoluminescence (PL) excitation profile for (11,3) tubes.

[Fig. 4(c)].

In summary, we produced chirality-selective excitations of coherent RBM oscillations in SWNTs by implementing multiple pulse trains with repetition rates matched to specific RBM frequencies. We obtained single-chirality information for many tube chiralities and extracted detailed information about the phase and modulation of the absorption, leading to an experimental confirmation that the lattice initially expands in response to the pump pulse. Also, the probe energy dependence of the differential transmission is satisfactorily described by RBM-induced band gap modulations, and analysis of the amplitude further proves coherent phonon spectroscopy to be a type of modulation spectroscopy. Beyond providing a powerful tool in accessing fundamental properties of

the material, the technique presented here may lead to chirality-selective end functionalization and tube filling via CP-driven end cap opening [18, 24].

We thank the Korean Research Foundation (MOEHRD, Basic Research Promotion Fund, KRF-2006-311-C00056), the Korea Science and Engineering Foundation (R11-2008-095-01000-0), the Robert A. Welch Foundation (C-1509), and NSF (DMR-0134058 and DMR-0325474) for support. We thank J. Shaver for technical assistance.

* kye@gnu.ac.kr; corresponding author.

† kono@rice.edu; corresponding author.

- [1] A. Jorio, G. Dresselhaus, and M. S. Dresselhaus, eds., *Carbon Nanotubes: Advanced Topics in the Synthesis, Structure, Properties and Applications* (Springer, Berlin, 2008).
- [2] M. J. O'Connell, ed., *Carbon Nanotubes: Properties and Applications* (CRC Press, Boca Raton, 2006).
- [3] M. S. Dresselhaus, G. Dresselhaus, and P. Avouris, eds., *Carbon Nanotubes: Synthesis, Structure, Properties, and Applications* (Springer, Berlin, 2001).
- [4] S. M. Bachilo *et al.*, J. Am. Chem. Soc. **125**, 11186 (2003).
- [5] M. S. Arnold, S. I. Stupp, and M. C. Hersam, Nano Lett. **5**, 713 (2005).
- [6] C.-M. Yang *et al.*, J. Phys. Chem. B **109**, 19242 (2005).
- [7] Y. Miyata, Y. Maniwa, and H. Kataura, J. Phys. Chem. B **110**, 25 (2006).
- [8] M. S. Arnold *et al.*, Nature Nanotechnol. **1**, 60 (2006).
- [9] A. M. Weiner, J. P. Heritage, and E. M. Kirschner, J. Opt. Soc. Am. B **5**, 1563 (1988).
- [10] A. M. Weiner and D. E. Leaird, Opt. Lett. **15**, 51 (1990).
- [11] T. Laarmann *et al.*, Phys. Rev. Lett. **98**, 058302 (2007).
- [12] Y. S. Lim *et al.*, Nano Lett. **6**, 2696 (2006).
- [13] A. Gambetta *et al.*, Nature Physics **2**, 515 (2006).
- [14] M. J. O'Connell *et al.*, Science **297**, 593 (2002).
- [15] A. M. Weiner *et al.*, Science **247**, 1317 (1990).
- [16] K. G. Lee *et al.*, Phys. Rev. B **74**, 113201 (2006).
- [17] M. Hase *et al.*, Appl. Phys. Lett. **69**, 2474 (1996).
- [18] T. Dumitrică *et al.*, Phys. Rev. B **74**, 193406 (2006).
- [19] D. Porezag *et al.*, Phys. Rev. B **51**, 12947 (1995).
- [20] J.-W. Jiang *et al.*, Phys. Rev. B **73**, 235434 (2006).
- [21] For more details, see G. D. Sanders *et al.*, arXiv:0812.1953v1 [cond-mat.mes-hall].
- [22] M. Cardona, *Modulation Spectroscopy* (Academic Press, New York, 1969).
- [23] H. L. Fragnito, J.-Y. Bigot, P. C. Becker, and C. V. Shank, Chem. Phys. Lett. **160**, 101 (1989).
- [24] T. Dumitrică *et al.*, Phys. Rev. Lett. **92**, 117401 (2004).